LAWRENCE
LIVERMORE
NATIONAL
LABORATORY

UCRL-JRNL-220097

Six-fold Coordinated Carbon Dioxide VI

V. Iota, C.-S. Yoo, J.-H. Klepeis, Z. Jenei

March 24, 2006

Nature Materials

Six-fold Coordinated Carbon Dioxide VI

Valentin Iota, Choong-Shik Yoo*, Jae-Hyun Klepeis, Zsolt Jenei,
William Evans, and Hyunchae Cynn

Lawrence Livermore National Laboratory, Livermore, CA 94551, USA.

Under standard conditions, carbon dioxide (CO_2) is a simple molecular gas and an important atmospheric constituent while silicon dioxide (SiO_2) is a covalent solid, and represents one of the fundamental minerals of the planet. The remarkable dissimilarity between these two group IV oxides is diminished at higher pressures and temperatures as CO_2 transforms to a series of solid phases, from simple molecular to a fully covalent extended-solid V, structurally analogous to SiO_2 tridymite. Here, we present the discovery of a new extended-solid phase of carbon dioxide (CO_2): a six-fold coordinated stishovite-like phase VI, obtained by isothermal compression of associated CO_2-II[1,2] above 50GPa at 530-650K. Together with the previously reported CO_2-V[3-5] and a-carbonia[6], this new extended phase indicates a fundamental similarity between CO_2 – a prototypical molecular solid, and SiO_2 – one of Earth's fundamental building blocks. The phase diagram suggests a limited stability domain for molecular CO_2-I, and proposes that the conversion to extended-network solids above 40-50 GPa occurs via intermediate phases II,[1,2] III,[7,8] and IV.[9,10] The crystal structure of phase VI suggests strong disorder along the c-axis in stishovite-like $P4_2/mnm$, with carbon atoms manifesting an average six-fold coordination within the framework of sp^3 hybridization.

Carbon dioxide is a prototypical molecular system, with strong covalent bonds within the O=C=O molecules and rather weak quadrupolar interactions between them. At high pressures and temperatures, CO_2 transforms to a series of solid polymorphs with differing intermolecular interactions, chemical bonding and crystal structures (Fig. 1). Phase V, in particular, consists of a network of corner sharing CO_4 tetrahedra, structurally similar to SiO_2 tridymite. Thus, CO_2-V is a fundamentally new material that exhibits extremely low compressibility[5] and strong optically nonlinearity[3]. The large disparity in

chemical bonding between the extended network and molecular CO_2 results in a broad metastability domain for phase V, to room temperature and almost to ambient pressure.[3,5]

The other CO_2 phases, II,[1,2] III[7,8] and IV[9-11] (formed in the intermediate pressure-temperature regime) exhibit strong intermolecular interactions, enhanced substantially over those of typical quadrupolar molecular solids[12]. The strong interactions lead to enhanced collective behavior of molecules, and result in strong associations of neighboring molecules in phase II, strain-induced disorder in phase III, and molecular bending in phase IV. Accordingly, these phases have been considered as intermediates between the simple molecular phase I and the fully extended phase V.

The crystallographic similarities between CO_2 and SiO_2 polymorphs[2,5,10,13] suggest the existence of other CO_2 extended solids, including six-fold stishovite. The strong covalence in C-O bonds and the rigidity of sp^3- bond angles, however, appear to hamper the formation of six-fold coordinated carbon units[14]. Total-energy calculations predict four-fold cristoballite[14] and/or layered carbonate[4] structures to be among the most stable configurations, while six-fold CO_2 are thought to stabilize only at ultra-high pressures above 400GPa[15].

In this letter, we report the discovery of fully extended stishovite-like CO_2 phase VI, formed at pressures below 100GPa (Fig. 1). Based on a large number of resistive- and laser-heating experiments using membrane-diamond anvil cells (mDACs), we propose the relationship between the molecular and extended phases in the pressure-temperature domain shown in Fig. 1.

CO_2-VI is obtained by isothermal compression of phase II to pressures above 50GPa at temperatures 530-650 K. As shown in Fig. 2, the most notable Raman feature of CO_2-VI is the emergence of a strong band around 1010cm^{-1} at 50GPa. This mode frequency is substantially higher than that of four-fold coordinated carbon in CO_2-V (~800cm^{-1})[3], indicating it likely originates from six-fold coordinated carbons in octahedral sites – similar to the A_{1g} mode of stishovite.[16] Following this assignment, we further associate the peaks at 300cm^{-1} to B_{1g}, 680cm^{-1} for E_g, and a weak, but measurable band at 1100cm^{-1} to B_{2g}, thus accounting for all four Raman-active modes reported in stishovite.[16] Importantly, the frequencies of these modes scale very well to those

observed in SiO_2 polymorphs (see Table I). In addition, in Figure 3 we compare the observed Raman spectra of CO_2-VI with those of other Group IV dioxides in rutile structures. We find that the frequencies of all four Raman-active modes scale linearly with the reduced mass, strongly supporting the present assignment of phase VI as stishovite-like. The data for SiO_2, GeO_2, and SnO_2 are from previous studies.[17]

Figure 4 summarizes the pressure dependence of the Raman modes of the new material. In addition to the four modes assigned to the stishovite-like structure, we observe a number of broad Raman features in CO_2-VI, centered at ~2000, 950, and 700cm^{-1} at 65GPa, which we assign to disorder in the stishovite structure. In fact, the 950 and 700cm^{-1} Raman bands are very similar to those of amorphous CO_2.[6] While the 2000cm^{-1} band is well within the overtone range of the A_{1g} band, we note that the C-O stretching mode of carbosonium[18] or a theoretically suggested ring dimer[19] also appear in this frequency range.

The II-to-VI transition is strongly affected by kinetics, requiring slow compression over several hours in a wide pressure range. While the conversion to CO_2-VI initiates at ~50GPa (530K), residual CO_2-II is observable to 60-65GPa. In this pressure range, the A_{1g} mode of phase VI gradually increases while the E_g mode of phase II gradually decreases in intensity and eventually disappears above 60-65GPa, as shown in Fig. 2. CO_2-VI can also be produced by isobaric heating of phase III to ~700-900K above 50GPa, although this method typically leads to a less crystalline phase. Once CO_2-VI is formed at high pressures and temperatures, it remains stable in a wide pressure range, from 90GPa (the maximum pressure applied in the present study), down to 20GPa, below which it transforms back to phase II. CO_2-VI is also stable in a wide temperature range from ambient to at least 1200 K at 50GPa, the maximum temperature reached in our resistive heating experiments. Further heating CO_2-VI to above 1500K using Nd:YLF laser converts the sample to CO_2-V (Fig. 2).

The stability of six-fold coordinated carbon dioxide at around 50GPa is remarkable. It has not been reported in any other carbon compounds, and theory has predicted its existence only at substantially higher pressures above 400GPa at 0K.[15] We attribute its low pressure stability to the crystal structure of phase II[2] in which each

carbon atom already has six quasi-nearest neighbor oxygen atoms, facilitating the formation of the six-fold C-O single-bond configuration observed in phase VI. In fact, our x-ray diffraction data confirm the close similarity between the crystal structures of phase II and VI (Fig. 5).

Figure 5 shows the x-ray diffraction data of phase II and VI obtained as elevating pressures at 600 K. Phase II diffraction pattern is well described in terms of stishovite-like $P4_2/mnm$; a=3.5430(5)Å c=4.1544(7)Å, C:2a(0,0,0) and O:2f(x,x,0) x=0.247(1). Small differences observed in the 110 and 101 reflections represent a minor, less than 0.1 %, lattice distortion in the ab- plane.[2]

Fig. 5 shows a remarkable similarity between the diffraction patterns of phases II and VI, confirming the structural similarity between the two phases. Indeed, the diffraction patterns of phase VI are reasonably well refined in terms of the same space group $P4_2/mnm$; a=3.4284(3){3.363(1)}Å, c=4.0259(7){3.973(4)}Å at 59{70}GPa. Furthermore, all observed pressure-induced diffraction changes occur smoothly and continuously across the phase transition. Two most characteristic changes are a gradual diminution of the 002/111 intensity ratio and an overall broadening of all reflection lines. However, in $P4_2/mnm$ carbon atoms in the 2(a) sites can contribute only to the hkl reflections matching h+k+l=2n, while oxygen atoms in the 4(f) do not have any additional reflection conditions. Therefore, to describe the observed diffraction changes in phase VI, it is necessary to introduce the movement of atomic positions away from the ab-plane, by either allowing carbon atoms to deviate from 2a(0,0,0) along the c-axis to 4e(0,0,z) (shown in Fig. 5 inset) or oxygen atoms from 4f(xx0) to 8m(xxz) or more generally 16k(xyz) (not shown), reducing the atomic occupancy correspondingly. In this model, we found that the value of the displacement z increases gradually above 50GPa, approaching z=0.095{0.170} at 59{70}GPa (see, Sfig. 1 inset). This results in all carbon atoms well within carbon-oxygen single-bond distances, 1.45-1.71Å, with six quasi-nearest oxygen atoms in a highly distorted octahedral configuration as illustrated in Fig. 5 inset.

Alternately, the observed diffraction changes may also be described in terms of large-amplitude thermal vibrations. The best refinements of the x-ray data in Fig. 5a, however, result in relatively large thermal displacement parameters; 0.16(1){0.110(8)} $Å^2$ for carbon and 0.11(1){0.096(8)} $Å^2$ for oxygen at 59{70} GPa, two-three times of those previously obtained in phase II at the similar temperatures. Therefore, we prefer the static disorder model described above, with the fixed initial displacement parameters at 0.058 Å2 for both C and O. Nevertheless, we found that the later refined thermal displacement parameters become again larger; 0.109(8) Å at 59 GPa and 0.115(7) Å at 70 GPa or actual thermal motion of ~0.33-0.34 Å. These values are quite comparable to the displacement of carbon atoms along the c-axis, 0.4-0.6 Å (see, Fig. 5b). In this regard, it is difficult to differentiate the static disorder from the dynamic thermal model. In either case, carbon atoms remain on average six-fold coordinated with oxygen atoms.

While the present x-ray data confirms the stishovite-like $P4_2/mnm$ structure for phase VI, there is a subtle difference from stishovite. That is, the CO_6 octahedron in phase VI is made of two edge-sharing CO_4 units that share single carbon atom. Nevertheless, the similarity in the Raman spectra between phase VI and stishovite clearly indicates that up to 90GPa the amount of disorder is relatively small to maintain an average coordination of six. The short interatomic oxygen-oxygen contact distance in the *ab*-plane of phase II, 2.1-2.4Å depending on the P,T conditions, is well in the repulsion regime and thus leads to the mechanical instability[14,20] and the observed structural frustration upon pressure increase. This results in a configuration of carbon atoms manifesting six-fold coordination while maintaining the frame work of sp^3 hybridization at elevated pressures.

We point out that the proposed disordered $P4_2/mnm$ model cannot be uniquely determined based on the limited number of reflections observed in the present powder x-ray diffraction patterns. Nevertheless, in addition to its close similarity to the parent phase II, the present model is consistent with all our other experimental observations. First, it explains the increased ionicity of C-O bonds in phase VI, as observed in the Raman spectra and also predicted by theory.[15] Second, it accounts for the significant temperature dependence of the specific volume of phase VI (see, Sfig. 1). At 70GPa, the

specific volume of phase VI is 0.305cm^3/g at 600 K but collapses to ~0.290-0.220cm^3/g at 300K, well within the range of fully extended solids (for example, 0.265cm^3/g for phase V at 300K).[5] Third, the proposed structural disorder is consistent with the emergence of the broad Raman bands in phase VI (marked as "*dis*" in Figs. 2 and 4). Finally, it provides a mechanism for the stability of phase VI at moderate pressures and temperatures (above 50GPa and 550K), in contrast to the extreme pressures (400GPa) predicted by theory.[15]

Finally, considering the rich abundance of carbon, oxygen and silicon in the Earth's mantle, the new high-density form of six-fold carbon dioxide may offer new concepts in geo- and mineral-chemistry. For example, CO_2 could exist in the Earth mantle as four- and six-fold covalent solids and within alloys or solid solutions with SiO_2 and/or other minerals. The structural similarities between CO_2 and SiO_2 polymorphs would presumably enhance their mutual solubility and chemical reactivity at the pressure-temperature conditions of the Earth's mantle. The structural instability of 6-fold CO_2 at low pressures and its enhanced ionic character upon decompression, would help account for the carbonate minerals originating from the Earth's interior[21] as well as for the high-temperature origin of carbonates in Martian Meteorites.[22]

References

1. Iota, V. and Yoo, C. S. Phase Diagram of Carbon Dioxide: Evidence for a New Associated Phase *Phys. Rev. Lett*. **86**, 5922–5925 (2001);

2. Yoo, C. S. et al., Crystal structure of pseudo-six-fold carbon dioxide phase II at high pressures and temperatures. *Phys. Rev. B* **65**,104103 (2002).

3. Iota, V., Yoo, C. S., and Cynn, H., Quartzlike Carbon Dioxide: An Optically Nonlinear Extended Solid at High Pressures and Temperatures. *Science* **283,** 1510-1513 (1999).

4. Sera, S., Corazon, C., Chiarotti, G.L., Scandolo, S., and Tossatti, E., Pressure-Induced Solid Carbonates from Molecular CO_2 by Computer Simulation. *Science* **284**, 788-790 (1999)

5. Yoo, C.S., et al. Crystal Structure of Carbon Dioxide at High Pressure: "Superhard" Polymeric Carbon Dioxide. *Phys. Rev. Lett.* **83**, 5527-5530 (1999).

6. Santoro, M., Gorelli, F.A., Bini, R., Ruocco, G., Scandolo, S., and Crichton, W.A., Amorphous silica-like carbon dioxide, *Nature* **441**, 857-860 (2006).

7. Aoki, K., Yamawaki, H., Sakashita, M., Gotoh, Y., and Takemura, K., Crystal structure of the high-pressure phase of solid CO_2, *Science* **263**, 356-358 (1994).

8. Olijnyk, H. and Jephcoat, A.P., Vibrational studies on CO_2 up to 40 GPa by Raman spectroscopy at room temperature. *Phys. Rev. B* **57**, 879-888 (1998).

9. Yoo, C. S., Iota, V., and Cynn, H., Nonlinear Carbon Dioxide at High Pressures and Temperatures. *Phys. Rev. Lett*. **86**, 444–447 (2001);

10. Park, J.-H. et al. , Crystal structure of bent carbon dioxide phase IV. *Phys. Rev. B* **68**, 014107 (2003)

11. Gorelli, F.A., Giordano, V.M., Salvi, P.R. and Bini, R. Linear Carbon Dioxide in the High-Pressure High-Temperature Crystalline Phase IV. *Phys. Rev. Lett*. **93**, 205503 (2004).

12. Kuchta, B. and R. Etters, R., Generalized free-energy method used to calculate the high-pressure, high-temperature phase transition in solid CO_2. *Phys. Rev. B* **47**,

14691–14695 (1993).

13. Sinclair, W. and Ringwood, A. E. Single crystal analysis of the structure of stishovite. *Nature (London)* **272**, 714-715 (1978).

14. Dong, J., et al., Investigation of hardness in tetrahedrally bonded nonmolecular CO_2 solids by density-functional theory. *Phys. Rev. B* **62**, 14685–14689 (2000).

15. Holm, B., Ahuja, R., Belonoshko, A., and Johansson, B., Theoretical Investigation of High Pressure Phases of Carbon Dioxide *Phys. Rev. Lett*. **85**, 1258–1261 (2000).

16. Hemley, R.J., Mao, H.K., Chao, E.C.T., Raman spectrum of natural and synthetic stishovite, *Phys. Chem. Minerals* **13**, 285-290 (1986).

17. Mammone J.F., Nicol, M. and Sharma, S. K., Raman spectra of TiO_2-II, TiO_2-III, SnO_2, and GeO_2 at high pressure *J. Phys.Chem. Solids* **42**, 379 (1981)

18. C.S. Yoo, High Pressure Chemistry of Molecular Solids: Evidence for Novel Extended Phases of Carbon Dioxide, in *Science and Technology of High Pressure*, edited by M. H. Manghnani, W.J. Nellis, and M. F. Nicol, Vol 1, p 86-89 (Univ. Press, Hyderabad, India, 2000)

19. Tassone, F., Chiarotti, G.L., Rousseau, R., Scandolo, S. and Tosatti, E. Dimerization of CO_2 at High Pressure and Temperature. *ChemPhysChem* **6**, 1752-1756 (2005).

20. Cohen, R. E., First-principles predictions of elasticity and phase transitions in high pressure SiO_2 and geophysical implications. *High Pressure Research: Application to Earth and Planetary Sciences*, edited by Y. Syono and M. H. Manghnani, p 425 (Terra Scientific, AGU, Washington DC, 1992)

21. Santillan, J. and Williams, Q. A high-pressure infrared and X-ray study of $FeCO_3$ and $MnCO_3$: comparison with $CaMg(CO_3)2$-dolomite. *Physics of the Earth and Planetary Interiors*, **143-144**, 291-304 (2004).

22. Harvey, R.P. and Mcsween, H.Y. A possible high-temperature origin for the carbonates in the martian meteorite ALH84001 *Nature* **382**, 49-51 (1996)

Supplementary Information is linked to the online version of the paper at www.nature.com/nature.

Acknowledgements. The work has been supported by the LDRD and PDRP programs at the LLNL, University of California under the auspices of the U.S.-DOE under contract number W-7405-ENG-48. The x-ray work was done by using the High Pressure Collaborating Acess Team's (HPCAT) micro-diffraction beamline (16IDB) of the Advanced Photon Source. Use of the HPCAT facility was supported by DOE-BES, DOE-NNSA (CDAC, LLNL, UNLV), NSF, DOD-TACOM, and the W. M. Keck Foundation.

Author Information. The authors declare no competing financial interests. Correspondence and requests for materials should be addressed to C-S.Y. at yoo1@llnl.gov or V.I. at iota1@llnl.gov.

Table 1: Comparison of the major Raman frequencies observed in extended CO_2 phases and corresponding SiO_2 polymorphs in four and six-fold configurations. The numbers indicate the Raman shift in cm^{-1} at ambient pressure, obtained by the extrapolation of the bands in Fig. 4 for CO_2 phases and from Ref. 16 for SiO_2 phases**.**

Four-fold		Six-fold	
SiO_2	CO_2-V	SiO_2	CO_2-VI
464	660	967	1051
206	285	753	905
128	240	589	620
		231	285

Figure captions:

Fig. 1 Phase diagram of carbon dioxide illustrating the molecular to nonmolecular phase transitions to four- and six-fold coordinated carbon atoms. The arrows represent two typical experimental paths: isothermal compression of phase II to 90 GPa or isobaric heating of phase III to 1200 K, shown together with the observed phase transformations. Phase V was synthesized by laser-heating the quenched phase VI well above ~1500 K (marked as dashed line). The dash-dot lines between phase II and III indicates a kinetic line, while the broken melting line of phase IV was not measured. The grey, blue and red colors in the figure, respectively, signify the stability fields of molecular, intermediates, and extended phases and the electron delocalization occurring gradually in CO_2, *via* the intermediate phases II and IV.

Fig. 2 Raman spectra of carbon dioxide phases at high temperatures and pressures, representing the phase transition from strongly associated phase II to fully extended, stishovite-like phase VI at 600K and 51GPa. Note that residual phase II (marked by *) still apparent at this pressure gradually weakens and eventually disappears above ~65GPa, while the features of phase VI are enhanced. CO_2-VI is quenchable at ambient temperature, and laser-heating the quenched phase VI to above 1500K transforms it to CO_2-V.

Fig. 3 Pressure-dependence of the Raman modes observed in the extended phases of CO_2-VI (in blue) and V (in black from Ref. 3), overlaid with those of CO_2-II (in green) for comparison. The broad features arising from the disorder in phase VI are also shown (in dark blue, labeled as "*dis*"). Open and solid symbols signify the data obtained during pressure upstroke and downstroke, respectively.

Fig. 4 Raman mode frequencies of CO_2-VI compared of with those of other Group IV dioxides in rutile structures. We find a near-linear scaling of the four principal Raman bands with the reduced mass, strongly supporting our stishovite-like assignment for phase VI.

Fig. 5 Structural model for CO_2-VI based on in situ X-ray diffraction measurements (a) Angle-dispersive x-ray diffraction patterns of CO_2-II and VI (blue plus symbols), shown together with the refined (red lines) and difference (green lines) patterns. The x-ray wavelength was 0.3682 Å, and the hkl reflection lines are also marked. (b) Crystal structures of phase II and VI in a stishovite-like $P4_2/mnm$ structure. Note that carbon atoms in phase VI are disordered but maintain an average six-fold coordination within the carbon frame work of sp^3 hybridization

Experimental methods:

Samples were loaded into an externally heated He-gas membrane-diamond anvil cell (mDAC) by condensing 99.99% pure CO_2 gas at 10 MPa and 233K in a sealed pressurized vessel. The use of resistively heated mDACs provided precise control over both pressure up to (+/- 2 GPa up to 100 GPa) and temperature (+/- 10K up to 1200K). Furthermore, the mDAC applies a constant load by He-gas to the sample during external heating to 1200 K at a given pressure thus allowing isobaric heating experiments. The precise control over the experimental pressure-temperature path was crucial considering the significant metastability observed in CO_2 phases. The sample temperature was measured by a K-type thermocouple attached in close proximity to the diamond-anvil, and the pressure was determined by measuring the R_1 luminescence of several micron-size rubies (Al_2O_3:Cr) placed around the sample. We performed in-situ Raman measurements using both 514.5nm and 488.8nm lines of an Ar+ laser. For laser-heating experiments, we used the 1054nm line of Nd:YLF laser to heat the CO_2 samples indirectly by heating either the ruby or the Re gasket edge as an absorber.

Angle-dispersive x-ray diffraction (ADXD) data were obtained at the microdiffraction beamline of the HPCAT (High Pressure Collaborative Acess Team) at the APS (Advanced Photon Source) by using focused (~0.01-0.02 μm) monochromatic x-rays (λ = 0.3682 Å) and a high-resolution image plate detector. The recorded two-dimensional diffraction images (Debye-Scherrer's rings) were then integrated to produce high quality ADXD patterns using FIT2D and analyzed with the XRDA and GSAS programs.

Supplementary figures captions:

Sfig. 1 The specific volumes of CO_2 phases plotted as a function of pressure for comparison. In the inset, the 600K-structural parameters of carbon and oxygen atoms are also plotted to illustrate the rapid increase above the phase II-to-VI phase transition at 50 GPa. Note the large temperature dependence of the specific volume of phase VI, originating from the disorder in carbon atoms at elevated temperatures. Because of large disorder in the diffraction pattern of quenched phase VI, the specific volumes are estimated based only on a broad 111 reflection, to illustrate the range between the lower limit $^{LL}VI_{300K}$ in isotropic compression and the upper limit $^{UL}VI_{300K}$ in anisotropic compression along the c-axis.

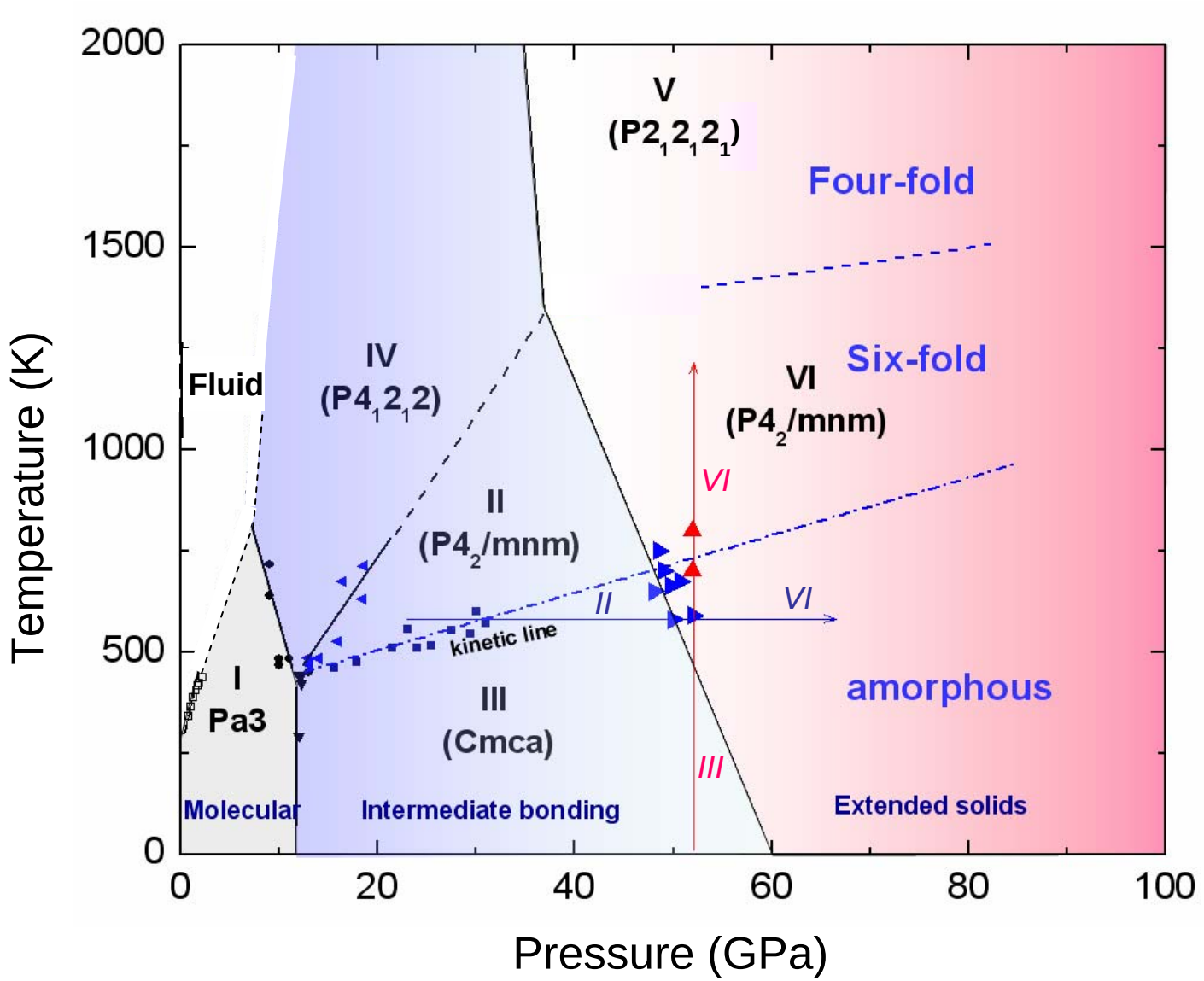
2000
1500
1000
500
0
0
20
40
60
80
100
Temperature (K)
Pressure (GPa)
V
(P2$_1$2$_1$2$_1$)
Four-fold
Six-fold
Fluid
IV
(P4$_1$2$_1$2)
VI
(P4$_2$/mnm)
II
(P4$_2$/mnm)
VI
II
VI
kinetic line
I
Pa3
III
(Cmca)
III
amorphous
Molecular
Intermediate bonding
Extended solids

Fig. 1

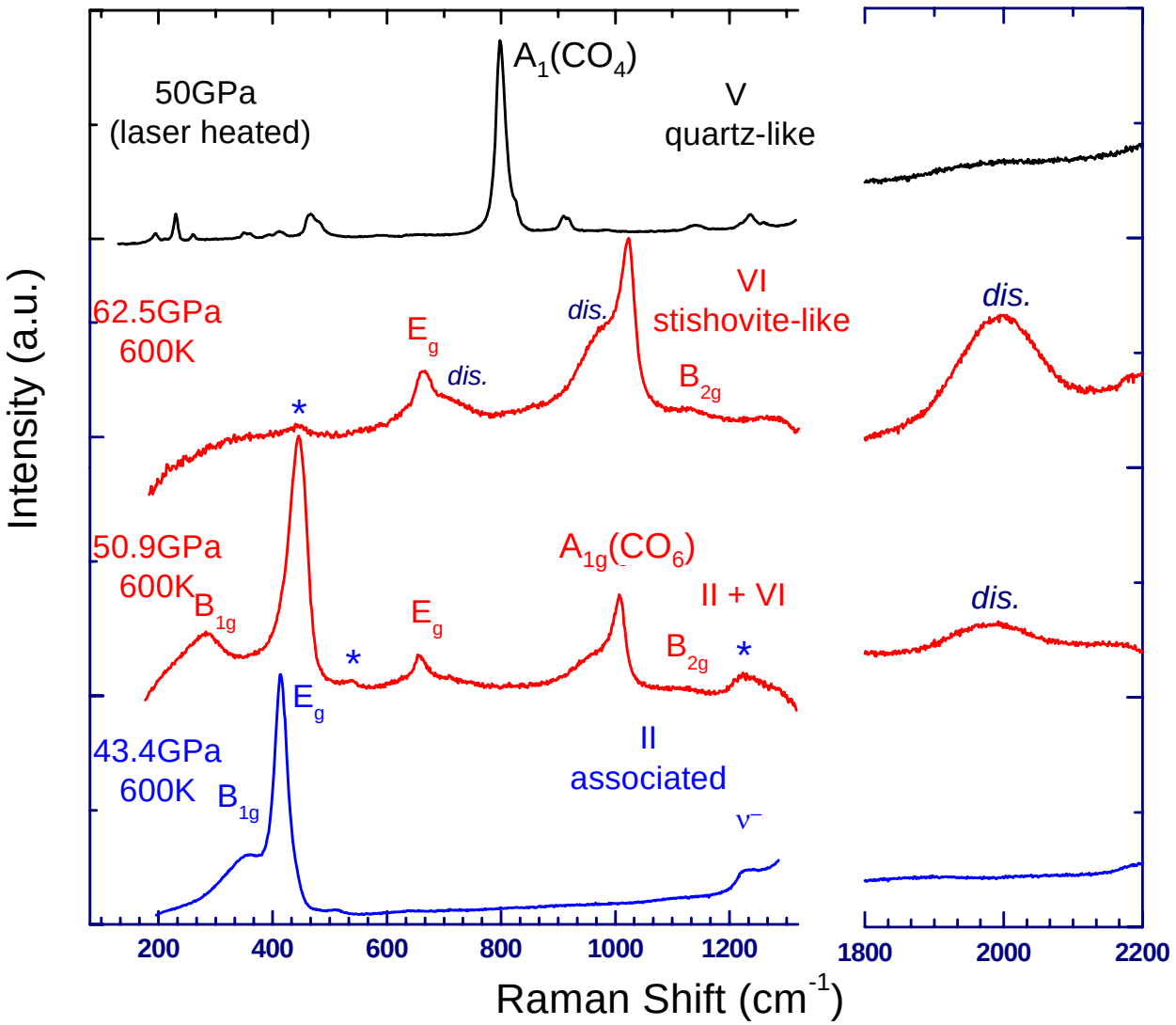
A1(CO4)
50GPa
(laser heated)
V
quartz-like
62.5GPa
600K
Eg
dis.
dis.
VI
stishovite-like
B2g
*
50.9GPa
600K
B1g
A1g(CO6)
II + VI
Eg
B2g
*
*
Eg
43.4GPa
600K
B1g
II
associated
ν⁻
dis.
dis.
Intensity (a.u.)
200
400
600
800
1000
1200
1800
2000
2200
Raman Shift (cm-1)

Fig. 2

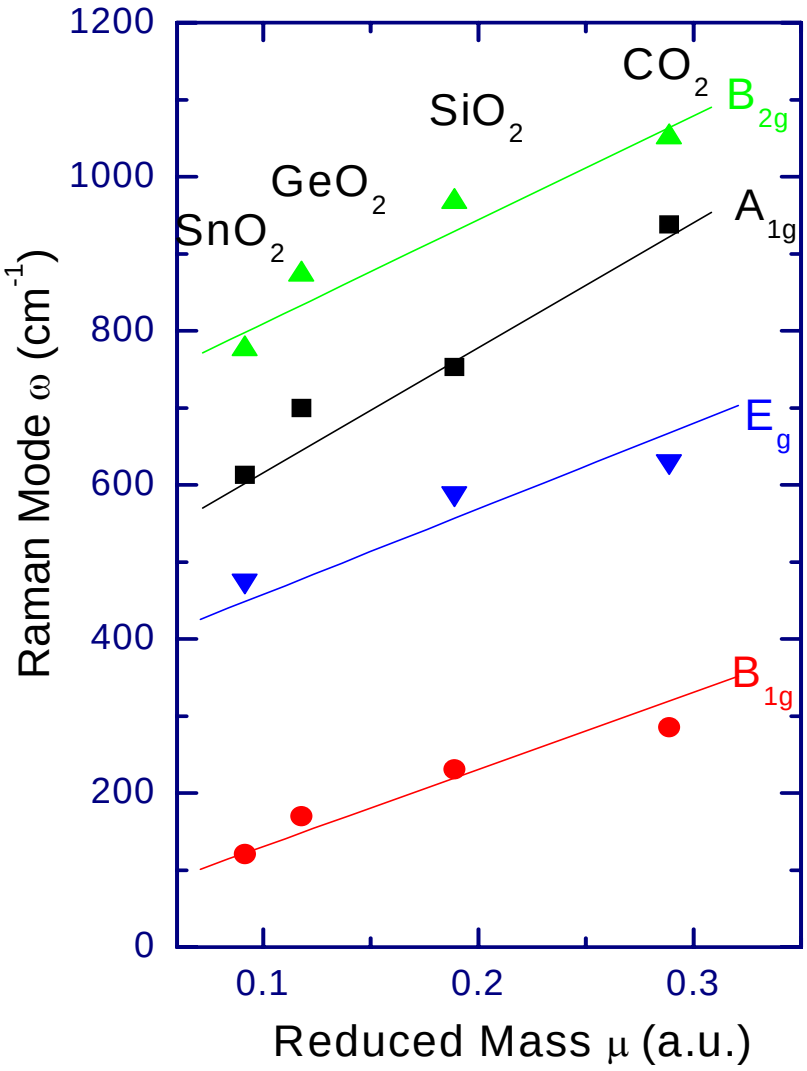
1200
1000
800
600
400
200
0
0.1
0.2
0.3
Raman Mode ω (cm-1)
Reduced Mass μ (a.u.)
CO2
SiO2
GeO2
SnO2
B2g
A1g
Eg
B1g

Fig. 3

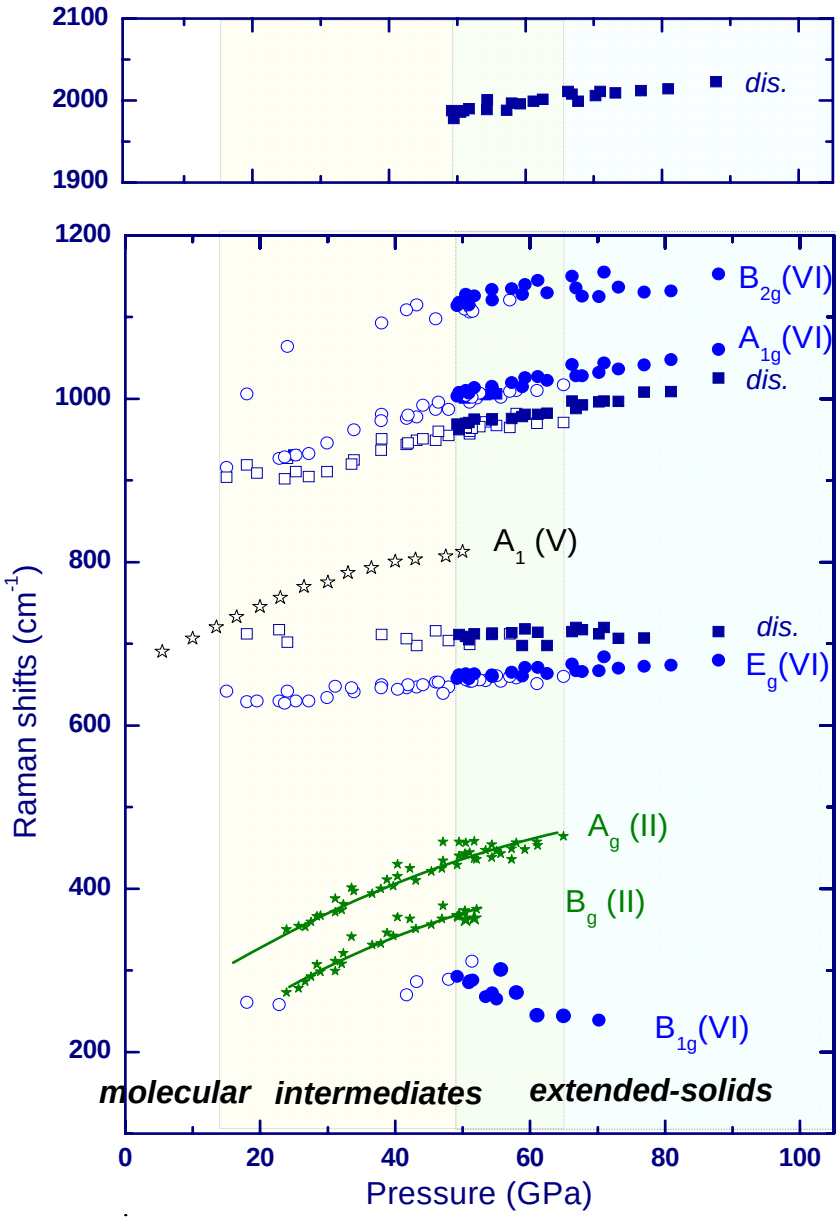
2100
2000
1900
dis.
1200
1000
800
600
400
200
B2g(VI)
A1g(VI)
dis.
A1 (V)
dis.
Eg(VI)
Ag (II)
Bg (II)
B1g(VI)
molecular
intermediates
extended-solids
Raman shifts (cm-1)
0
20
40
60
80
100
Pressure (GPa)

Fig. 4

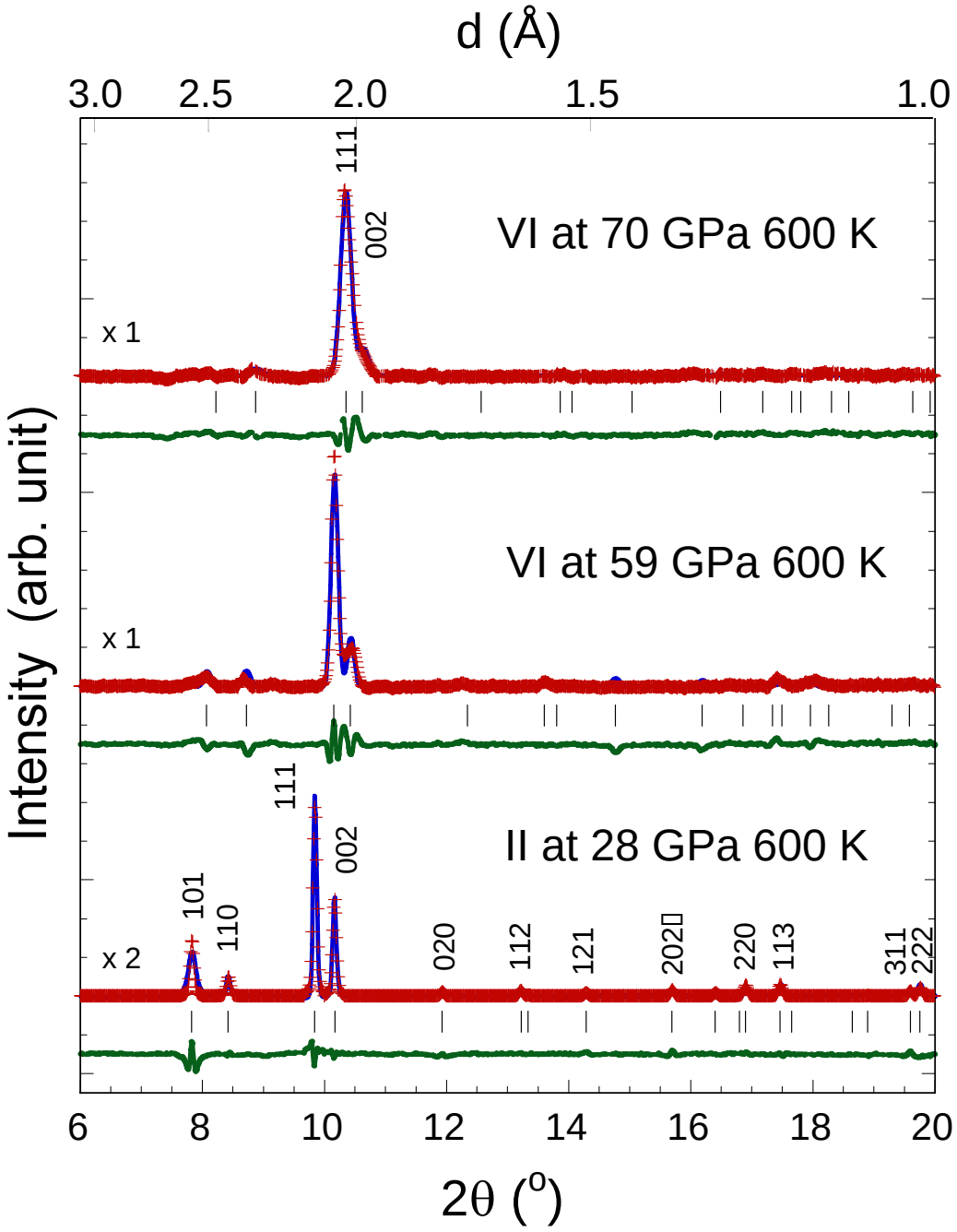
d (Å)
3.0
2.5
2.0
1.5
1.0
111
002
VI at 70 GPa 600 K
x 1
VI at 59 GPa 600 K
x 1
111
002
101
110
II at 28 GPa 600 K
x 2
020
112
121
202
220
113
311
222
Intensity (arb. unit)
6
8
10
12
14
16
18
20
2θ (°)

Fig. 5 (a)

CO_2-II

CO_2-VI

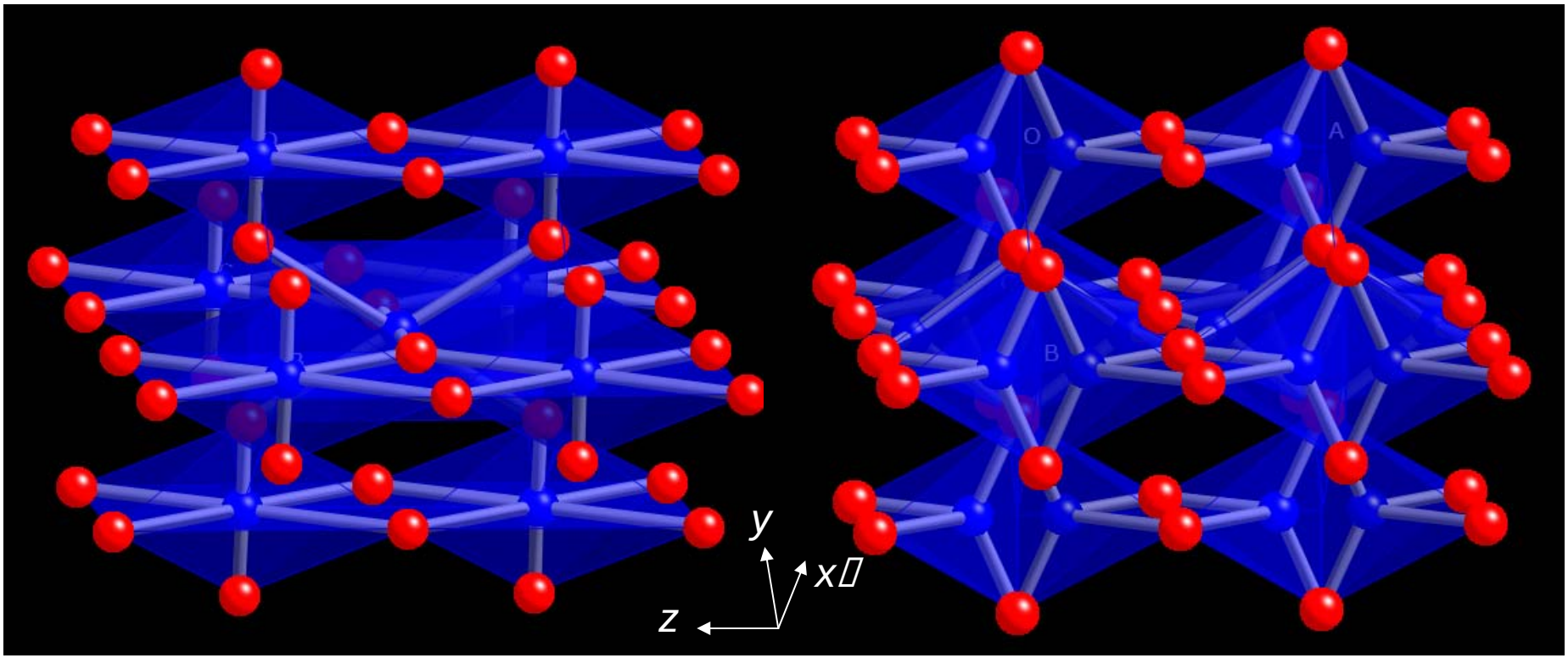

28 GPa and 600 K

59 GPa and 600 K

Fig. 5(b)

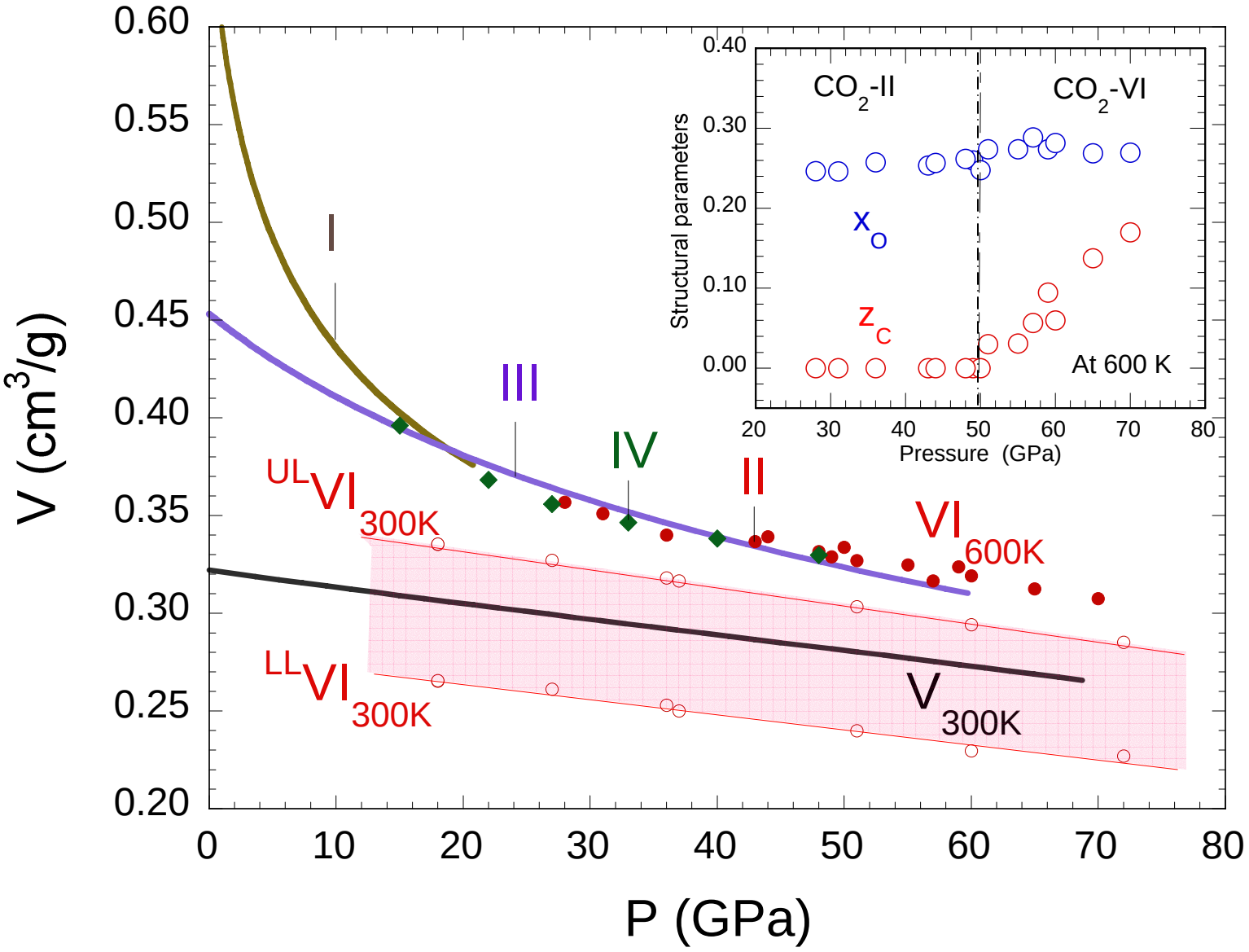
V (cm3/g)
P (GPa)
I
III
IV
II
ULVI300K
LLVI300K
VI600K
V300K
Structural parameters
CO2-II
CO2-VI
xO
zC
At 600 K
Pressure (GPa)

Sfig. 1